Journal of The Electrochemical Society, **155** (1) J7-J10 (2008)
0013-4651/2007/155(1)/J7/4/$23.00 © The Electrochemical Society

The Effect of Mg Incorporation on Structural and Optical Properties of Zn_2GeO_4:Mn Phosphor

G. Anoop,* K. Mini Krishna, and M. K. Jayaraj[z]

Optoelectronic Devices Laboratory, Department of Physics, Cochin University of Science and Technology, Kochi-682 022, India

The effect of Mg incorporation on structural and optical characteristics of rhombohedral Zn_2GeO_4 doped with manganese was systematically studied, fixing the concentration of manganese at 2 atom %. The phosphors were prepared by a high-temperature solid-state-reaction technique. The structural properties were studied using X-ray diffraction (XRD) and optical properties were characterized by diffuse reflectance spectra (DRS), photoluminescent excitation (PLE), and photoluminescent (PL) emission spectra. The XRD and DRS analyses reveal that Mg can be successfully alloyed in $Zn_{1.96-1.96x}Mg_{1.96x}GeO_4$:$Mn_{0.04}$ up to $x = 0.30$ and forms a solid solution. The PL emission was maximum when 5 atom % Zn was replaced with Mg in comparison to an Mg-free $Zn_{1.96}GeO_4$:$Mn_{0.04}$ sample. The mechanism of luminescence is identified as resonant transfer from a subbandgap state in the host to Mn^{2+}. The PLE and DRS spectra of $Zn_{1.96-1.96x}Mg_{1.96x}GeO_4$:$Mn_{0.04}$ ($0 \leqslant x \leqslant 0.5$) exhibited a blue shift with an increase in Mg concentration. The cell volume was found to be a monotonously increasing function of Mg concentration up to $x = 0.25$, beyond which it varied randomly.
© 2007 The Electrochemical Society. [DOI: 10.1149/1.2799585] All rights reserved.

Manuscript submitted June 13, 2007; revised manuscript received September 12, 2007. Available electronically October 31, 2007.

Thin-film electroluminescent devices are mostly based on sulfide phosphors (ZnS, SrS, etc).[1-4] Recently, oxide phosphors[5,6] have been considered as potential substitutes due to their extreme stability in vacuum, moisture insensitivity, and nondegradation under electron bombardment. Several oxide phosphor hosts like $ZnGa_2O_4$, Zn_2GeO_4, Zn_2SiO_4, Y_2O_3, etc., have been extensively studied.[7-15] Among them, Zn_2GeO_4 doped with Mn is an excellent green-emitting phosphor. Rhombohedral Zn_2GeO_4 is similar to Zn_2SiO_4 but has a lower crystallization temperature. Thin films of Zn_2GeO_4:Mn^{2+} grown using radio frequency (rf) magnetron sputtering and pulsed laser deposition techniques also show good luminescent characteristics.[13-15] The green emission in Zn_2GeO_4:Mn^{2+} is due to the transitions in $3d^5$ electrons of Mn^{2+} that substitute tetrahedral Zn^{2+} sites.[13] Several methods can be adopted to enhance the luminescent properties of these phosphors. Codoping is one such efficient approach. In Zn_2GeO_4, codopants that substitute Ge^{4+} and Zn^{2+} can provide positive results. Among the various ions (Mg^{2+}, Cd^{2+}, Ba^{2+}, etc.) that can replace Zn^{2+} in Zn_2GeO_4, Mg^{2+} is a better choice because its ionic radius is more comparable with Zn^{2+} than other ions. In the present work, the effect of Mg^{2+} codoping on structural and luminescent properties of Zn_2GeO_4:Mn is studied in detail.

Experimental

The samples were prepared by conventional high-temperature solid-state reaction of constituent oxides, namely, ZnO (Alfa Aesar 99.99%), MgO (Alfa Aesar 99.99%), and GeO_2 (Alfa Aesar 99.999%). Manganese was added in the form of manganous acetate [$Mn(CH_3COO)_2$]. The powders were mixed stoichiometrically in ethanol medium and calcined in air at 1200°C for 12 h in a tube furnace to obtain $Zn_{1.96-1.96x}Mg_{1.96x}GeO_4$:$Mn_{0.04}$ (x was varied from 0 to 0.5). All samples were doped with 2 atom % of Mn, which was the optimized concentration of Mn in $Zn_{2-2x}GeO_4$:Mn_{2x} phosphor which has maximum photoluminescence (PL) emission intensity. The crystal structure of the powder phosphors were analyzed using X-ray powder diffraction (XRD) using Cu Kα radiation (Rigaku, Japan). The diffuse reflectance spectra (DRS) were recorded to analyze the bandgap using a Jasco V-570 spectrophotometer with an integrating sphere attachment. The reference used was $BaSO_4$. The room-temperature photoluminescent emission (PL) and excitation (PLE) spectra were recorded using Spex Fluoromax-3 spectrofluorimeter equipped with a 150 W xenon lamp in the range 200–800 nm. The Zn/Ge atomic ratio was measured using energy-dispersed X-ray analysis (EDX) with a JEOL JSM 6490 scanning electron microscope. The relative luminescence quantum efficiency (QE) of phosphor was measured using a standard lamp phosphor, $BaMgAl_{10}O_{17}$ (BAM), of known quantum efficiency (90%). For the calculations, integrated PL intensity of BAM and phosphors were measured at identical conditions such as sample weight, instrument settings, temperature, and excitation wavelength (300 nm).

Results and Discussion

Figure 1 shows the XRD patterns of $Zn_{1.96-1.96x}Mg_{1.96x}GeO_4$:$Mn_{0.04}$ ($0 \leqslant x \leqslant 0.5$). The standard spectra of undoped Zn_2GeO_4 (JCPDS card no. 11-0687) is plotted for reference. The XRD pattern clearly implies that Mg is randomly substituting Zn in $Zn_{1.96}GeO_4$:$Mn_{0.04}$ for concentrations up to $x = 0.25$, forming a single phase and preserving the hexagonal symmetry of the host lattice. No traces of constituent oxides were found in the diffraction patterns. The peaks other than that of Zn_2GeO_4 were identified to be of orthorhombic Mg_2GeO_4 (JCPDS card no. 36-1479). But above $x = 0.25$, phase segregation commences, limiting the solid solubility of Mg in $Zn_{1.96}GeO_4$:$Mn_{0.04}$. In wurtzite $Zn_{1-x}Mg_xO$, Mg is found to be soluble up to $x = 0.33$.[16-18] As the crystal structures of Zn_2GeO_4 (rhombohedral) and Mg_2GeO_4 (orthorhombic) are different, substitution of Zn with Mg does not

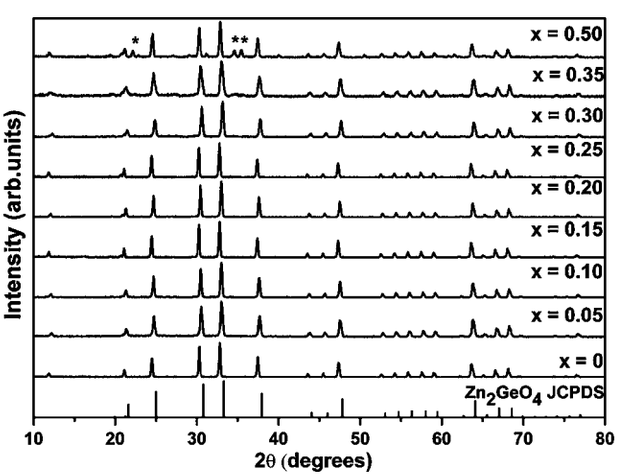

Figure 1. XRD patterns of $Zn_{1.96-1.96x}Mg_{1.96x}GeO_4$:$Mn_{0.04}$, $0 \leqslant x \leqslant 0.5$. * represents peaks of Mg_2GeO_4.

* Electrochemical Society Student Member.
[z] E-mail: mkj@cusat.ac.in

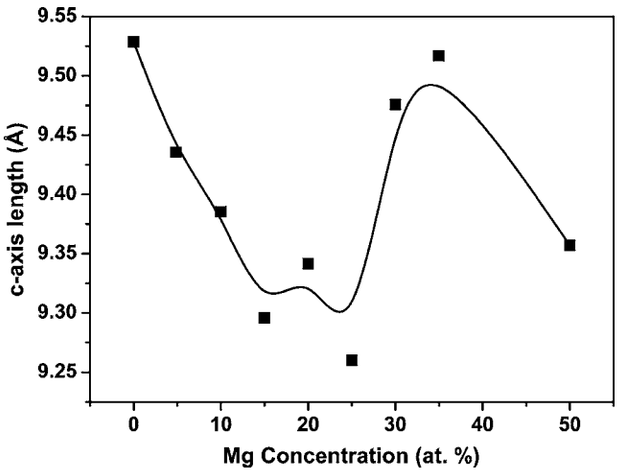

Figure 2. Variation of *c*-axis length with Mg concentration.

occur for all concentrations and results in phase separation. Alloying is observed up to $x = 0.25$ and the lattice constants of $Zn_{1.96-1.96x}Mg_{1.96x}GeO_4:Mn_{0.04}$ are expected to change as Zn^{2+} and Mg^{2+} have different ionic radii (0.60 and 0.57 pm, respectively) for four coordination.[19]

The *c*-axis length and cell volume was calculated from the observed XRD data,[20] the variation of which with Mg concentration is shown in Fig. 2 and 3, respectively. The *c*-axis length of Zn_2GeO_4 is 9.53 Å and that of Mg_2GeO_4 is 4.91 Å. The *c*-axis length shows a contraction with increased Mg substitution up to $x = 0.25$. But for $x = 0.30$, 0.35, and 0.5, *c*-axis length increases. This is because as Mg concentration increases, simple substitution of Mg terminates and starts to segregate into different phases. However, cell volume increases continuously up to $x = 0.25$ and decreases for $x = 0.30$, 0.35, and 0.5, which is due to an elongation in the *a* parameter up to $x = 0.25$. The difference in cell volume is assumed to be due to the difference in ionic radii of Zn^{2+} and Mg^{2+}, which also gives rise to a difference in *c*-axis length.

The variation of full width at half-maximum (fwhm) of the (410) XRD peak with Mg concentration is plotted in Fig. 4. There is gradual variation in the fwhm value up to $x = 0.25$, which indicates Mg alloying in the Zn_2GeO_4 lattice. However, it shows a sudden increase at $x = 0.30$ and 0.35, for which phase segregation takes place, and for $x = 0.5$ it again decreases. The substitution of Mg at

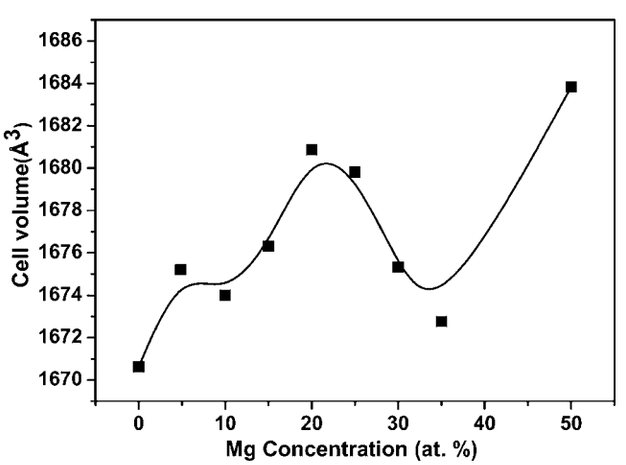

Figure 3. Variation of cell volume with Mg concentration.

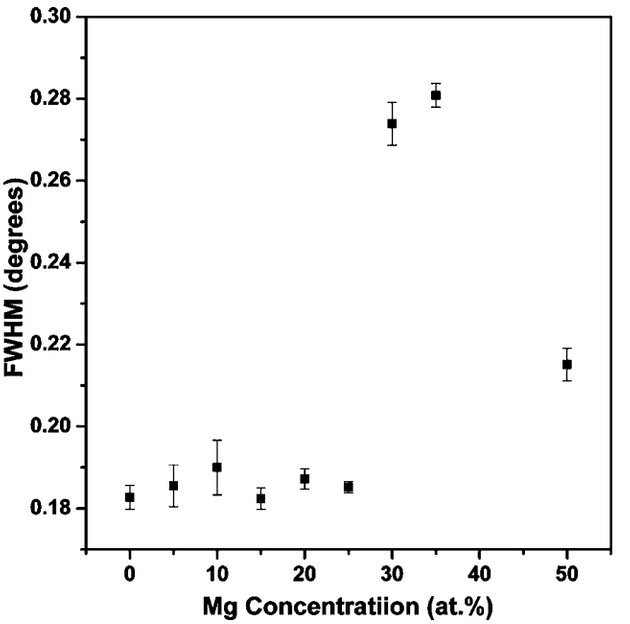

Figure 4. Variation of fwhm with Mg concentration.

Zn sites is expected to broaden the XRD peak and, interestingly, maximum broadening is observed for $x = 0.35$ at which phase segregates.

The *c*-axis length, cell volume, and fwhm show almost similar behavior with Mg substitution. A sudden change at $x = 0.30$ and 0.35 is observed for all parameters which is due to the inbuilt strain caused by Mg substitution in the lattice. Because of this strain, phase segregates, and above $x = 0.35$ Zn_2GeO_4 and Mg_2GeO_4 is separately formed; beyond $x = 0.35$ these parameters randomly approach the previous value for which solid solution exists. Therefore, it can be concluded from the XRD studies that phase segregation occurs due to the inbuilt strain in the lattice due to Mg substitution and that Mg replaces Zn substitutionally.

Figure 5a shows the DRS spectra of $Zn_{1.96-1.96x}GeO_4:Mn_{0.04}$ for the various Mg concentrations and the variation of bandgap with Mg concentration. As the Mg doping percentage increases, the absorption edge blue-shifts. The bandgap of pure Zn_2GeO_4, $Zn_{1.96}GeO_4:Mn_{0.04}$, and $Zn_{1.96-1.96x}Mg_{1.96x}GeO_4:Mn_{0.04}$ samples were calculated from the $[(k/s)h\nu]^2$ vs $h\nu$ plots, where k and s denote the absorption and scattering coefficients, respectively. The bandgap of pure Zn_2GeO_4 is found to be 4.57 eV and that of Mn-doped Zn_2GeO_4 is 3.44 eV (Fig. 5b). The reduced bandgap for the $Zn_{1.96}GeO_4:Mn_{0.04}$ sample is due to the formation of subbandgap states (discussed later). In the normal case Mg^{2+} replaces Zn^{2+} in $Zn_{1.96}GeO_4:Mn_{0.04}$, but there is a limit to this simple substitution because Zn_2GeO_4 (rhombohedral) and Mg_2GeO_4 (orthorhombic) crystallizes into different crystal structures. Therefore, the substitution of Mg^{2+} at Zn^{2+} sites creates strain in the lattice due to the reduced size of Mg^{2+}, which results in the blue shift of the absorption edge.

Figure 6 shows PL emission spectra of $Zn_{1.96-1.96x}Mg_{1.96x}GeO_4:Mn_{0.04}(0 \leqslant x \leqslant 0.5)$. PL emission intensity is found to increase for $x = 0.05$, 0.10, 0.15, and 0.20 and decrease beyond $x = 0.25$ compared to the undoped sample, the maximum being observed for the sample doped with 5 atom % Mg ($x = 0.05$). The green luminescence at 535 nm is observed from $^4T_1 \rightarrow {}^6A_1$ transitions of $3d^5$ electrons of Mn^{2+}, which substitutes the tetrahedrally coordinated Zn^{2+} ions in rhombohedral Zn_2GeO_4, as the host provides only tetrahedral sites for substitution.[14] When Mg is codoped in $Zn_{1.96}GeO_4:Mn_{0.04}$, luminescent intensity

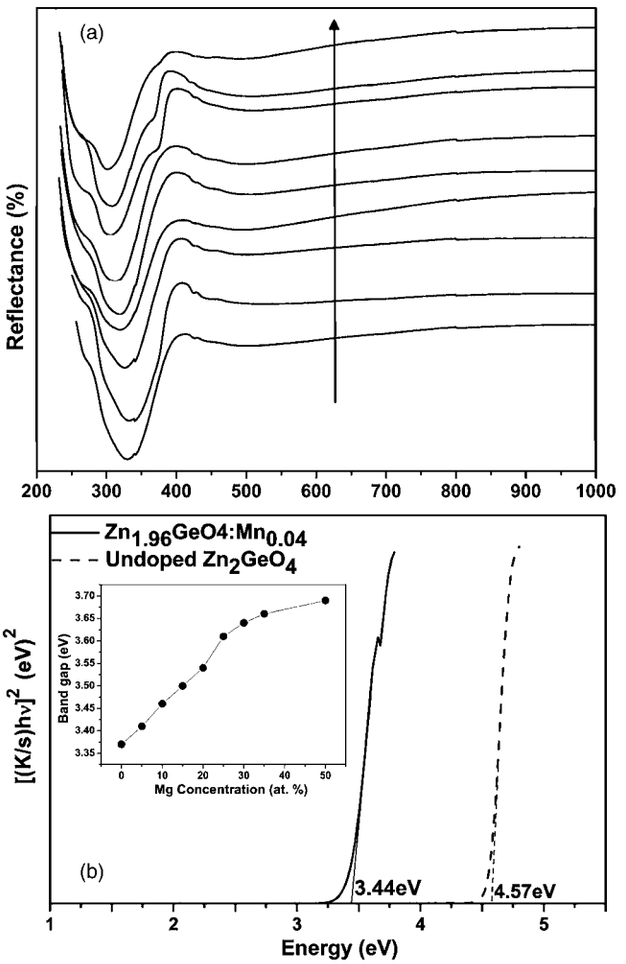

Figure 5. (a) The DRS spectra of $Zn_{1.96-1.96x}GeO_4:Mn_{0.04}$, Mg (arrow indicates x variation from 0 to 0.5 in steps of 0.05, final one being $x = 0.5$). (b) Bandgap of pure Zn_2GeO_4 and $Zn_{1.96}GeO_4:Mn_{0.04}$. Inset shows the variation in bandgap with Mg concentration.

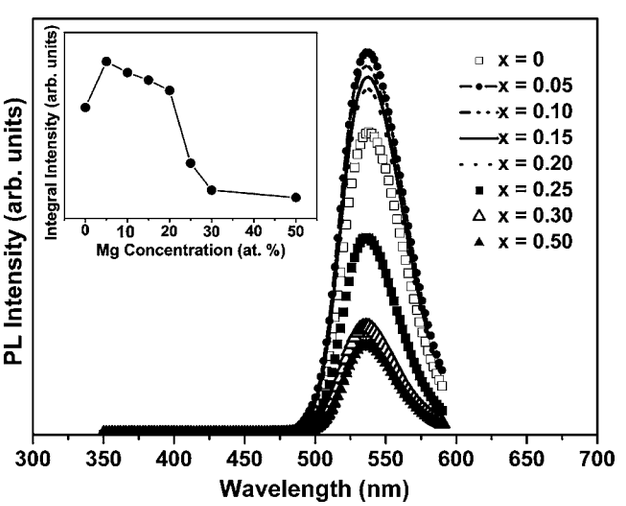

Figure 6. PL emission spectra of $Zn_{1.96-1.96x}Mg_{1.96x}GeO4:Mn_{0.04}$ ($0 \leqslant x \leqslant 0.5$), $\lambda_{exc=}$300 nm. Inset shows variation in integral intensity with respect to Mg concentration.

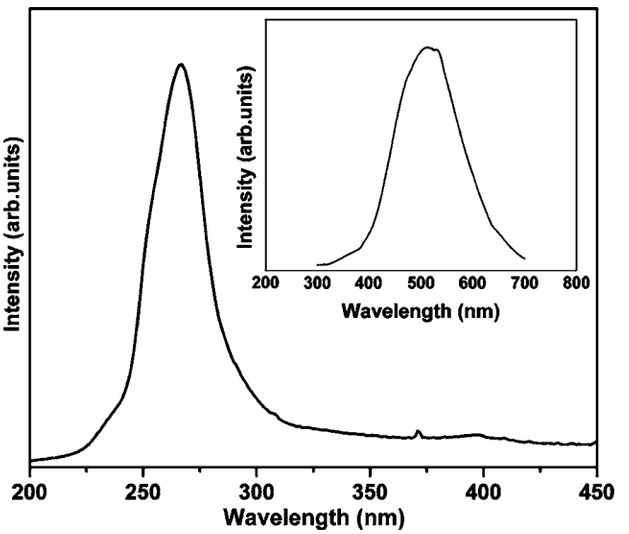

Figure 7. PLE spectra of pure Zn_2GeO_4 monitored at 507 nm. Inset shows the emission spectra when excited at 266 nm.

varies due to the change in effective crystal field of tetrahedrally coordinated Mn^{2+} ions. When Mg^{2+} is incorporated in the lattice it creates excited state energy levels (consisting of 3s and 3p) near the excited state of Mn^{2+} [comprising of $^4T_1(^4G)$, $^4T_2(^4G)$, $^4A_1(^4G)$, and $^4T_1(^4P)$, shown later]. Therefore, transition from the Mg levels to ground state of Mn^{2+} becomes more permissible, because the transition is more spin allowed compared to $3d^5$ transitions of Mn^{2+}.[21] However, when concentration of Mg is increased, luminescent intensity decreases because effective transfer of charge via excited states of Mg does not take place due to inbuilt strain in the lattice. The quantum efficiency of the phosphor ($Zn_{1.862}Mg_{0.098}GeO_4:Mn_{0.04}$) that showed maximum luminescent intensity is 41%, relative to BAM phosphor.

Figure 7 shows excitation and emission spectra of undoped Zn_2GeO_4. Undoped Zn_2GeO_4 shows absorption at 266 nm with a shoulder at 251 nm for emission at 507 nm. Pure Zn_2GeO_4 shows a broad emission from 300 to 650, peaking at 507 nm when excited with 266 nm. But when Mn^{2+} is added the emission becomes narrow and shifts to 535 nm and excitation maximum shifts to 335 nm in addition to 266 nm (bandedge) and 285 nm (direct excitation of Mn^{2+}) absorption, indicating the presence of a subbandgap. The green luminescence from the undoped sample is a signature of intrinsic defect levels in the lattice during its synthesis.

Figure 8 shows PL excitation spectra of $Zn_{1.96}GeO_4:Mn_{0.04}$ and the inset shows a variation of PLE peak wavelength with respect to the Mg concentration. PLE shifts to a lower wavelength as Mg concentration is increased, which is consistent with the results obtained from DRS spectra. The spectra shows a shoulder at 285 nm, while the peak wavelength is at 335 nm for the $x = 0$ sample. The shoulder at 285 nm and peak at 425 nm is evidently direct excitation of tetrahedrally coordinated Mn^{2+} ions.[22]

The bottom of the conduction band of Zn_2GeO_4 is comprised of Ge 4p orbitals, with a small contribution from Zn 4s and 4p orbitals, and the upper part of the valence band is composed of O 2p levels.[23] The mechanism for the emission at 535 nm is identified as band-to-band absorption and nonradiative transfer to a center, from which resonant transfer to activator takes place. This center lies nearly 1 eV below the conduction band and is likely to be an oxygen defect which is also observed in the DRS spectra (Fig. 5). This can be formed via migration of octahedrally coordinated Ge^{4+} ions to tetrahedral-position-forming Ge^{3+} ions.[24] Because the vapor pressure of Zn is high and high-temperature solid-state reaction is employed for the phosphor synthesis, Zn evaporation takes place, leav-

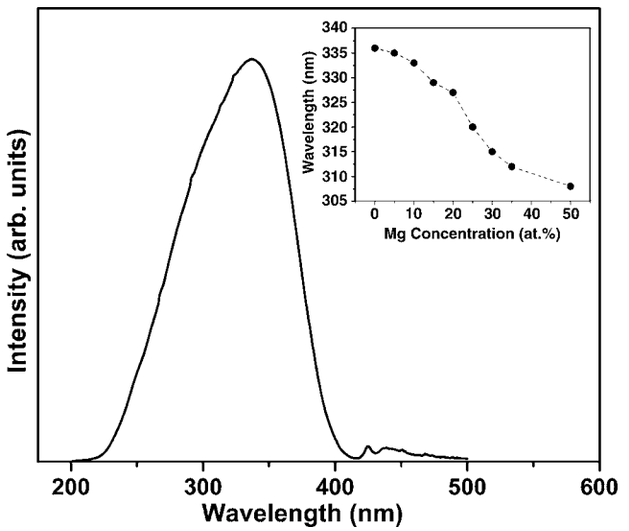

Figure 8. PLE spectra of $Zn_{1.96}GeO_4$: $Mn_{0.04}$. Inset shows variation of PL excitation with Mg concentration in Zn_2GeO_4:Mn.

ing behind a vacancy and thereby occupying Zn vacancy sites by Ge^{3+} ions migrated from the octahedral sites. This is also confirmed from EDX data. In all the samples, the cation (Zn/Ge) ratio was found to be less (1.3 for $x = 0$) than the actual value (1.96 for $x = 0$). In ZnO, a donor level 0.8 eV below the conduction band is observed, which gives rise to green luminescence and is created due to oxygen vacancy.[25] When Mn is added to the Zn_2GeO_4 host, it creates excited-state energy levels near this center in such a manner that the charge transfer to Mn takes place through absorption via this center along with band-to-band absorption (266 nm). Another possibility is Zn vacancy, which could form an acceptor level above the valence band. This is also observed in ZnO, where an acceptor level nearly 0.8 eV above the valence band is formed due to Zn vacancy.[25] But resonant transfer from a low-lying level to excited-state levels of Mn^{2+} is not possible. Another possibility is defect generated due to germanium. But that defect level is not perturbed by adding Mg, replacing Zn in the tetrahedral position. Because the ionic radii of Mg^{2+} and Ge^{4+} is not comparable, hardly a chance exists for Mg to replace Ge in Zn_2GeO_4. Therefore, this trap level could be due to oxygen deficiency. The energy levels and the mechanism of PL emission in Zn_2GeO_4:Mn is schematically represented in Fig. 9.

When Mg is added to the system, it creates energy levels near the excited-state levels of Mn^{2+} and also perturbs the V_O level, thereby shifting the absorption edge. Therefore, the DRS and PLE spectra show a blue shift when Mg is incorporated to Zn_2GeO_4:Mn host matrix.

Conclusion

In summary, Mg-doped $Zn_{1.96}GeO_4$:$Mn_{0.04}$ phosphor was prepared by solid-state reaction. The structural analysis reveals the formation of solid solution up to $x = 0.25$ in $Zn_{1.96-1.96x}Mg_{1.96x}GeO_4$:$Mn_{0.04}$. Beyond $x = 0.25$, phase segregation occurs. The absorption edge as observed from DRS and PLE spectra of Mn and Mg-doped samples indicates the presence of a subband-gap and was found to be blue shifted with an increase in Mg substitution. The PL emission spectra exhibits an increase in

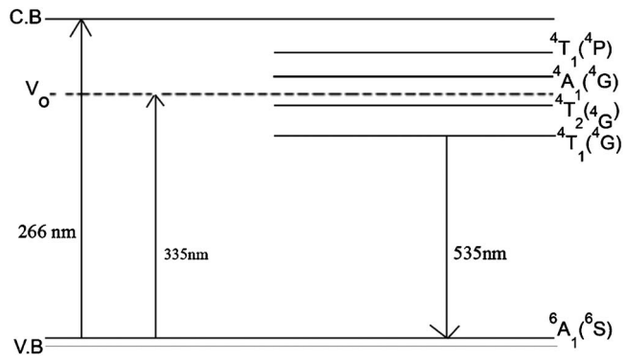

Figure 9. Energy-level scheme describing the excitation and emission mechanism of Zn_2GeO_4:Mn^{2+} phosphor.

luminescent intensity with Mg concentration at $x = 0.05$ in $Zn_{1.96-1.96x}Mg_{1.96x}GeO_4$:$Mn_{0.04}$ phosphor. The phosphor can be used as an active layer in ACTFEL devices.

Acknowledgments

This work was supported by the Department of Science and Technology of the Government of India. Author K.M.K. thanks CSIR for the grant of a fellowship. The authors thank S. Jayalekshmi and Rajive Tomy for their help during the sample preparation. Thanks are due to K. Manzoor for fruitful discussions and Sajin for EDX measurements.

References

1. C. B. Thomas and W. N. Cranton, *Appl. Phys. Lett.*, **63**, 3119 (1993).
2. M. K. Jayaraj and C. P. G. Vallabhan, *J. Electrochem. Soc.*, **138**, 1512 (1991).
3. K. Ohmi, K. Yamabe, H. Fukada, T. Fujiwara, S. Tanaka, and H. Kobayashi, *Appl. Phys. Lett.*, **73**, 1889 (1998).
4. B. A. Baukol, J. C. Hitt, P. D. Keir, and J. F. Wager, *Appl. Phys. Lett.*, **76**, 185 (2000).
5. T. Minami, *Solid-State Electron.*, **47**, 2237 (2003).
6. A. H. Kitai, *Thin Solid Films*, **445**, 367 (2003).
7. S. Itoh, H. Toki, Y. Sato, K. Morimoto, and T. Kishino, *J. Electrochem. Soc.*, **138**, 1509 (1991).
8. T. Minami, Y. Kuroi, T. Miyata, H. Yamada, and S. Takata, *J. Lumin.*, **72**, 997 (1997).
9. I. K. Jeong, H. L. Park, and S. I. Mho, *Solid State Commun.*, **108**, 823 (1998).
10. K. Mini Krishna, G. Anoop, and M. K. Jayaraj, *J. Electrochem. Soc.*, **154**, J310 (2007).
11. K. H. Hsu, M. R. Yang, and K. S. Chen, *J. Mater. Sci.: Mater. Electron.*, **9**, 283 (1998).
12. T. Minami, Y. Kuroi, and S. Takata, *J. Vac. Sci. Technol. A*, **14**, 1736 (1996).
13. L. C. Williams, D. Norton, J. Budai, and P. H. Holloway, *J. Electrochem. Soc.*, **151**, H188 (2004).
14. J. S. Lewis and P. H. Holloway, *J. Electrochem. Soc.*, **147**, 3148 (2000).
15. J. P. Bender, J. F. Wager, J. Kissick, B. L. Clark, and D. A. Keszler, *J. Lumin.*, **99**, 311 (2002).
16. T. H. Yeom, Y. H. Lee, T. S. Hahn, M. H. Oh, and S. H. Choh, *J. Appl. Phys.*, **79**, 1004 (1996).
17. A. Ohtomo, M. Kawasaki, T. Koida, K. Masabuchi, H. Koinama, Y. Sakurai, Y. Yoshida, T. Yasuda, and Y. Segawa, *Appl. Phys. Lett.*, **72**, 2466 (1998).
18. A. Ohtomo, M. Kawasaki, I. Ohkubo, H. Koinuma, T. Yasuda, and Y. Segawa, *Appl. Phys. Lett.*, **75**, 980 (1999).
19. R. D. Shannon, *Acta Crystallogr.*, **32**, 751 (1976).
20. B. D. Cullity and S. R. Stock, *Elements of X-Ray Diffraction*, 3rd ed., Prentice Hall, New York (2001).
21. K. S. Soha, B. Cho, H. Chang, and H. D. Park, *J. Electrochem. Soc.*, **146**, 2353 (1999).
22. L. Shea, R. K. Dutta, and J. J. Brown, Jr., *J. Electrochem. Soc.*, **141**, 1950 (1994).
23. J. Sato, H. Kobayashi, K. Ikarashi, N. Saito, H. Nishiyama, and Y. Inoue, *J. Phys. Chem.*, **108**, 4369 (2004).
24. V. Bondar, S. Popovich, T. Felter, and J. F. Wager, *Mater. Res. Soc. Symp. Proc.*, **667**, G761 (2001).
25. U. Ozgur, Y. I. Alivov, C. Liu, A. Teke, M. A. Reshchikov, S. Dogan, V. Avrutin, S. J. Cho, and H. Markoc, *J. Appl. Phys.*, **98**, 041301 (2005).